A Comprehensive Hepatitis C Viral Kinetic Model Explaining Cure

Eric Snoeck, Pascal Chanu, Marc Lavielle, Philippe Jacqmin, Niclas Jonsson, Karin Jorga, Timothy Goggin, Joseph Grippo, Shasha Jumbe, Nicolas Frey

HAL Id: hal-00637434

https://hal.archives-ouvertes.fr/hal-00637434

Submitted on 2 Nov 2011

1 **A comprehensive Hepatitis C viral kinetic model explaining *cure***

2

3 Eric Snoeck[1], Pascal Chanu[2], Marc Lavielle[3], Philippe Jacqmin[1], E. Niclas Jonsson[1],

4 Karin Jorga[2], Timothy Goggin[2], Joe Grippo[2], Nelson L. Jumbe[2], Nicolas Frey[2]

5

6 [1]Exprimo NV, Zwaanstraatje 4, B2800, Mechelen, Belgium. [2]F. Hoffmann-La Roche

7 Ltd., Grenzacherstrasse 124, 4070 Basel, Switzerland. [3]INRIA Saclay and Department

8 of Mathematics; University Paris-Sud, Orsay, France.

9

10 We propose a model that characterizes and links the complexity and diversity of

11 clinically observed Hepatitis C viral kinetics to sustained virologic response (SVR, the

12 primary clinical endpoint of Hepatitis C treatment defined as an undetectable viral load

13 at 24 weeks after treatment completion) in Chronic Hepatitis C (CHC) patients treated

14 with peginterferon α-2a ± ribavirin. New attributes of our Hepatitis C viral kinetic

15 model are- i) the implementation of a *cure*/viral eradication boundary, ii) employing all

16 HCV RNA measurements including those below the lower limit of quantification, and

17 iii) implementation of a population modeling approach. The model demonstrated

18 excellent positive (99.3%) and negative (97.1%) predictive values for SVR and high

19 sensitivity (96.6%) and specificity (99.4%). The proposed viral kinetic model provides a

20 framework for mechanistic exploration of treatment outcome, and permits evaluation of

21 alternative CHC treatment options to ultimately develop and test hypotheses for

22 personalizing treatments in this disease.

23

24   An estimated 170 million people or 2.1% of the world population are currently infected

25   with hepatitis C virus (HCV), which is more than four times the number of people

26   living with human immunodeficiency virus HIV (1). The current standard of care (SOC)

27   for Chronic Hepatitis C (CHC) patients is the combination of pegylated interferon α

28   with ribavirin (2,3). Successful HCV treatment outcome, i.e. sustained virologic

29   response (SVR), is when a patient's viral load is below the HCV RNA detection limit at

30   a follow-up evaluation 24-weeks following treatment completion. SVR rates of up to

31   66% have been obtained with the optimal regimen of peginterferon α-2a plus ribavirin

32   in treatment-naïve patients in large, randomized, multicentre trials (4,5). Patients

33   infected with the more difficult to treat HCV genotype 1 (G1), which represent about

34   70% of CHC patients in the US (6), are less likely to achieve an SVR than genotype

35   non-1 (Gn1) infected patients. Approximately 50% of HCV G1 infected patients

36   achieved an SVR when treated with peginterferon α-2a plus ribavirin, whereas

37   approximately 80% of HCV Gn1-infected patients achieved an SVR despite receiving a

38   shorter treatment duration and a lower ribavirin dose (5). Thus, HCV patients represent

39   a population with continued unmet medical need, having the potential to achieve a

40   higher SVR rate through optimized treatment approaches.

41   Modeling hepatitis C virus (HCV) dynamics during therapy has led to important

42   insights into the life cycle of HCV elucidating the kinetic parameters governing viral

43   infection and hepatocyte death, the antiviral effects of interferons, and how ribavirin

44   impacts HCV treatment (7). Models of HCV kinetics have provided a means to compare

45   different treatment regimens and outcomes in different patient populations (8). A model

46   of HCV infection was originally proposed by Neumann *et al.* (9) who adapted a model

47   of HIV infection (10,11). The Neumann model adequately describes typical short-term

48 therapy outcome characterized by an initial rapid viral decline followed by a second

49 slower decline until HCV RNA becomes undetectable (12,13). This model has therefore

50 been frequently used to describe viral load profiles after short-term treatment (8,14,15).

51 However, after current long-term SOC treatment, the virus is not eradicated in all CHC

52 patients (5). In the patients who do not achieve SVR (i.e the virus is not eradicated),

53 viral load either rebounds to pretreatment levels during therapy (*breakthrough*), or

54 returns to pretreatment levels upon cessation of therapy (*relapse*) (13). These two

55 phenomena, and crucially, an SVR cannot be described by the Neumann model (13),

56 and are the primary reason why early viral response does not uniformly predict the

57 clinical endpoint. Finally, and most importantly, previous analyses have used a naïve

58 method of handling the HCV RNA measurements below the lower limit of

59 quantification (LLOQ) by omission of all these measurements even though these values

60 contain critical information regarding long-term treatment outcome.

61 In this communication, we propose a novel approach of modelling the viral kinetics in

62 Hepatitis C. Firstly, a non-linear mixed effects model was developed by maximum

63 likelihood estimation (MLE) of the parameters using the extended stochastic

64 approximation expectation-maximization (SAEM) algorithm as implemented in the

65 *MONOLIX* software (16). Individual long-term HCV kinetic profiles of 2,100 CHC

66 patients treated with peginterferon α-2a alone or in combination with ribavirin using a

67 wide spectrum of dosing regimens were simultaneously described. Secondly, HCV

68 RNA measurements below the LLOQ were included. The proposed model permits the

69 distinction between SVR and LLOQ by including censored data residing between the

70 HCV RNA LLOQ and the irrevocable lower boundary of zero. Thirdly, *cure* or

71 complete virion eradication was determined from viral kinetics by implementation of a

72 viral eradication boundary. At the time point at which treatment drives the system to

73 less than one infected hepatocyte, the production of virions was set to zero. Modeling

74 results characterizing differences between patients having an SVR and those failing

75 treatment were explored in order to derive mechanistic hypotheses underpinning

76 treatment failure or success.

77

78 **RESULTS**

79 Parameters of the model were estimated with good precision (**Table 1**). The typical

80 value of the basic reproduction number R_0 was estimated to be 7.2 with an inter-

81 individual variability (IIV) of 137% CV. The relatively large IIV likely reflects the large

82 intrinsic biological difference in CHC disease. R_0 represents relative drug-effect

83 distance from the treatment intervention goal, which is to drive the reproduction number

84 during treatment (R_T) below 1 (**Supplementary** text note 2 online), in order to increase

85 the likelihood of attaining SVR (i.e. *cure*, defined as I < 1 infected hepatocyte).

86 Inspection of the individual parameter estimates in patients experiencing a breakthrough

87 during therapy indeed showed that the administered drug therapy failed to decrease the

88 reproduction number (R_T) below 1 (17,18). The maximum hepatocyte proliferation rate

89 (*r*) was 0.00562 day^{-1}, and simulations based on this *r* revealed that the predicted liver

90 regeneration matched well with the increase in original liver volume in 51 donors as

91 measured 1 year after providing right-lobe liver grafts [**Supplementary** text note 3

92 online (19)]. The typical value of the virion production rate *p* was 25.1 virions·day^{-1} and

93 the free virion clearance rate *c* was estimated to be 4.53 day^{-1}, corresponding to a free

94 virion half-life of 3.7 hours. This half-life lies within the previously reported range of

95 1.5-4.6 hours (12,13). Free virion clearance rate was found not to be influenced by HCV

96　genotype. In contrast, the infected cell death rate (δ) appeared to be dependent on HCV

97　genotype, and the typical value was estimated to be 0.139 day^{-1} in genotype-1 infected

98　patients and 0.192 day^{-1} in patients infected with HCV Gn1 (**Table 1**). These estimates

99　are in line with previously reported values of δ (20). The higher δ in HCV Gn1 infected

100　patients may indicate an enhanced immunological response and is in line with the

101　previous finding that a fast viral decay early in treatment correlates with SVR (20). Also

102　the typical value of the $ED_{50_{PEG}}$ was found to be lower in HCV Gn1 patients as

103　compared to patients infected with HCV G1, confirming the higher antiviral

104　effectiveness of peginterferon α-2a in blocking virion production in Gn1 patients

105　[**Table 1** and (20)]. The $ED_{50_{RBV}}$ was estimated to be 14.4 mg·kg^{-1}·day^{-1}, which

106　corresponds to rendering a fraction of 40-60% of the virions non-infectious for a

107　standard ribavirin treatment of 1,000/1,200 mg per day (see equation 6). The anti-viral

108　effect decay constant (K) was estimated to be 0.0238 day^{-1}, which corresponds to a half-

109　life of approximately 29 days. As the terminal half-life after multiple dosing of

110　peginterferon α-2a is approximately 160 h and that of ribavirin is approximately 12

111　days (21), the anti-viral effect decay constant may describe both pharmacokinetic and

112　pharmacodynamic processes. Finally, the variance of the residual error (σ^2) was

113　estimated to be 0.260. This residual error is relatively high but not uncommon for viral

114　kinetic models as a σ^2 of 0.38 was obtained previously in a similar analysis of HIV viral

115　load data (22).

116

117　**Model evaluation and qualification**

118　The goodness of fit assessment revealed that the individual viral load profiles are well

119　described by the model (**Supplementary** text note 4 online). Population based

120   diagnostics were also used, but are not easily interpretable unless simulated reference

121   graphs from the true model are used for comparison [**Supplementary** text note 4 online

122   (23)]. A selection of 12 individual viral load profiles shows that the HCV viral kinetic

123   model is able to not only describe the initial decreases in viral load over the first month,

124   but also the typical phenomena observed after longer-term therapy (**Figure 3**). The

125   model provided satisfactory positive (99.3%) and negative (97.1%) predictive values for

126   SVR combined with a high sensitivity (96.6%) and specificity (99.4%)

127   [**Supplementary** text note 5 online].

128   The predictive performance of the model was assessed by a model evaluation procedure

129   using the design and data of a large clinical trial not included in the model building

130   dataset (4). The model was successfully qualified for further simulations as the

131   predicted range of SVR rate in HCV G1 and Gn1 infected patients receiving 48 weeks

132   of treatment with peginterferon α-2a alone or in combination with ribavirin matched

133   well with the observed SVR rate in this study (**Figure 5**).

134

135   **Discussion**

136   The multi-dimensional interactions between HCV virus, host and drug are highly non-

137   linear and equilibrium outcomes quickly become counter-intuitive (24). Here, we

138   propose a population approach using MLE by the extended SAEM algorithm as

139   implemented in the *MONOLIX* software (16), to simultaneously describe individual

140   long-term HCV kinetic profiles of 2,100 CHC patients treated with peginterferon α-2a

141   alone or in combination with ribavirin. The four ordinary differential equations (ODE's)

142   of the HCV viral kinetic model (equations 1-4) were implemented in *MONOLIX*. HCV

143   viral kinetic models including ODE's have been previously used for exploratory

144 simulations (17,25), however not for simultaneously fitting the complexity and diversity

145 of clinically observed HCV viral kinetics.

146 The proposed model addresses the host-virus-drug interaction by advancing previously

147 known and novel ideas from a population perspective, simultaneously analyzing a wide

148 spectrum of treatment regimens (drug combinations, drug doses, schedule and treatment

149 durations), incorporating left-censored data previously largely excluded from analysis,

150 and implementing a viral eradication *cure* boundary to link viral kinetics to clinical

151 outcome (i.e. SVR). The final viral kinetic model was qualified using internal and

152 external datasets, including HCV G1 and Gn1 infected patients, and demonstrated

153 positive and negative predictive values as well as sensitivity and specificity exceeding

154 96%.

155 In clinical practice, milestone target treatment strategies, i.e., rapid virologic response

156 (RVR)- defined as attainment of undetectable HCV RNA level by week 4 of therapy

157 (26,27), or early virologic response (EVR)- defined ≥ 2 log reduction or undetectable

158 serum HCV RNA at week 12 of treatment, have been proposed to optimize SVR rates

159 by modifying treatment duration. However, these early treatment response landmarks

160 (regardless of time point) do not uniformly predict SVR because viral load either

161 rebounds to pretreatment levels during therapy (*breakthrough*), or returns to

162 pretreatment levels upon cessation of therapy (*relapse*). This observations leads to two

163 conclusions, (i) the relationship between RVR/EVR and SVR is correlative but not

164 prescriptive, and (ii) excluding HCV RNA measurements below the LLOQ (i.e., left-

165 censoring) likely biases SVR predictions. An extension of the SAEM algorithm as

166 implemented in the *MONOLIX* software handles left-censored data in nonlinear mixed-

167 effects models with computational efficiency (22). Comparison with classical methods

168 of handling missing data shows that the extended SAEM algorithm is less biased than

169 excluding subjects with censored measurements, omission of all censored data points,

170 and/or imputation to half the quantification limit for the first point below the LLOQ

171 with omission of subsequent missing data (28). Furthermore, the extended SAEM

172 algorithm has been demonstrated to be more efficient and/or less biased than

173 linearization or Monte Carlo approximation of the expectation step applied to censored

174 values (22).

175 The implementation of the *cure* boundary in the viral kinetic model is physiologically

176 based and consistent with the primary goal of HCV therapy, which is to completely

177 eradicate the virus. The final viral kinetic model was implemented as a two state system.

178 The ***off*** state (null virion production) was triggered when there was less than one

179 infected hepatocyte in the total plasma and extracellular fluid volume of distribution

180 thereby resulting in *cure*/SVR. The ***on*** state (constitutive virion production),

181 inadvertedly returns the patient to full blown disease when even a minute fraction of one

182 infected hepatocyte remains.

183 A comparison of the individual parameter estimates between patients with and without

184 an SVR reveals that R_0 and $ED_{50_{PEG}}$ are generally lower in SVR patients (**Figure 4**). A

185 relatively low R_0 prior to treatment and a relatively high inhibition of the virion

186 production increase the likelihood of $R_T < 1$ during treatment and will thus increase the

187 likelihood of SVR.

188 Inspection of the individual parameter estimates in patients experiencing a breakthrough

189 during therapy indeed showed that the administered drug therapy failed to decrease the

190 R_T below 1 (17,18). According to our modeling assumptions, a treatment with either

191 higher doses or a combination treatment with new drugs may be an option in these

192 patients in order to drive R_T below 1. The conditional explanation in patients relapsing

193 after the end of treatment may be twofold: i) on the one hand, relapsing patients may

194 have had a $R_T < 1$ during treatment, but were not treated long enough to cross the *cure*

195 boundary of $I < 1$ cell, so that the viral load quickly returned back to baseline at the end

196 of therapy, or ii) drug therapy may have failed to decrease the R_T below 1 (inadequate

197 efficacy). Extended treatment duration at the same drug combination, dose and schedule

198 in relapsing patients may therefore be an option in the former situation but not in the

199 latter. Based on these hypotheses, individual treatments may be optimized when the

200 individual R_0 and inhibition of the virion production are pre-determined or determined

201 early at treatment onset. The interplay between treatment duration, dose and schedule,

202 and/or sensitivity of hitting the *cure* boundary after high dose induction is yet to be fully

203 elucidated.

204 In our model-based analysis, the free virion clearance rate (*c*) did not appear to be a

205 prognostic factor for SVR (**Figure 4**), whereas the death rate of infected cells (δ) was

206 found to be generally higher in SVR patients indicating these patients may have an

207 enhanced immunological response and thus a higher likelihood of viral eradication.

208 Our proposed viral kinetic model is a simplification of the complex interaction between

209 host, infected hepatocytes, virus, and mechanisms of drug action and required fixing of

210 several liver physiology parameters to biologically justifiable values. Furthermore, the

211 combination of peginterferon α-2a and ribavirin is assumed to inhibit in a multiplicative

212 way the virion production (*p*) according to E_{max} dose-response relationships. While

213 some confidence in the predictive performance of the model is derived from the

214 qualification exercise described above, complete understanding of the implications of

215 these assumptions is not fully understood and should be further explored, particularly in

9

216   the case where the model would be used to explore the efficacy of new drugs in

217   combination with SOC. Another limitation of our current model is the fact that dose was

218   used as the pertubation to the system. Since HCV SOC pharmacotherapy has been

219   established through empirical study over a decade, investigation of schedule

220   dependence was not considered as primary to our objectives. This implies that a

221   pharmacokinetic model component will have to be added to the current model for the

222   evaluation of schedule dependence and/or adherence, especially for drugs with shorter

223   pharmacokinetic half-lives that are being developed.

224   In summary, our population HCV viral kinetic model was able to adequately describe

225   all individual long-term viral load profiles of 2,100 CHC patients receiving chronic

226   treatment of peginterferon α-2a alone or in combination with ribavirin. The model

227   provides new insights and explanations for typical phenomena observed in the clinic

228   such as breakthrough during therapy, relapse after stopping therapy and *cure* (or SVR).

229   Simulations based on our model may help to better understand current treatment success

230   and failure, and can also be used to predict and evaluate the efficacy of alternative

231   treatment options (e.g. alternative doses, durations and, with additional assumptions-

232   new drug combinations) in the overall CHC patient population. This will be described in

233   a follow-up communication. The proposed viral kinetic model provides a framework for

234   developing and testing hypotheses for evaluating new antiviral agents and personalizing

235   CHC treatments that would ultimately need to be validated in well designed clinical

236   trials.

237

238   **METHODS**

239   **Patients and Data**

240 Data from one phase-II study and four phase-III studies of peginterferon α-2a (40KD)

241 (Pegasys®) alone or in combination with ribavirin (Copegus®) were pooled. All patients

242 were required to have histologically and serologically proven CHC. The complete

243 inclusion and exclusion criteria, study design, and primary results have been published

244 elsewhere (5, 29-32). A total of 2,100 CHC patients were included in the final database.

245 Serum HCV RNA (COBAS AMPLICOR™ HCV Test, version 2.0) was measured at

246 specific time points during treatment and during the 24-week untreated follow-up

247 period. All available 21,284 HCV RNA measurements, of which 59% were below the

248 LLOQ, were modeled by accounting for the left-censoring in the analysis. The LLOQ of

249 the two different assays used were 50 IU/mL and 600 IU/mL (33).

250

251 **HCV viral kinetic model**

252 The viral kinetic model (equations 1-4) extends the original Neumann (9) model, to

253 include important contributions by Dahari *et al.* (density dependent proliferation of

254 hepatocytes [*r*], 17) and Pomfret *et al.* (hepatocyte intrinsic production, 19). Treatment

255 effect of peginterferon α-2a [*ε*] and the effect of ribavirin rendering a fraction of newly

256 produced virions non-infectious [*ρ*] (7) was implemented on the virion production rate

257 (*p*). The model structure of the viral kinetic model (**Figure 1**) is described by the

258 following mass balance equations:

259
$$\frac{dT}{dt} = s + r \cdot T \cdot \left(1 - \frac{T+I}{T_{max}}\right) - d \cdot T - \beta \cdot V_I \cdot T \tag{1}$$

260
$$\frac{dI}{dt} = \beta \cdot V_I \cdot T + r \cdot I \cdot \left(1 - \frac{T+I}{T_{max}}\right) - \delta \cdot I \tag{2}$$

261
$$\frac{dV_I}{dt} = (1-\rho) \cdot (1-\varepsilon) \cdot p \cdot I - c \cdot V_I \tag{3}$$

262 $$\frac{dV_{NI}}{dt} = \rho \cdot (1 - \varepsilon) \cdot p \cdot I - c \cdot V_{NI} \qquad (4)$$

263 where, infectious HCV virions (V_I) infect target cells (uninfected hepatocytes) [T],

264 creating productively infected cells (I) at a rate $\beta \cdot V_I \cdot T$. Uninfected hepatocytes are

265 produced at rate s and die at rate d. Infected hepatocytes die at rate δ. Similar to Dixit *et*

266 *al.* (7), it is assumed that infectious (V_I) and non-infectious (V_{NI}) virions are produced

267 from infected hepatocytes at rate p and cleared at rate c. The measured viral load (V) is

268 expressed in IU/mL, representing the sum of infectious and non-infectious virions $V =$

269 $V_I + V_{NI}$. The model was further extended with E_{max} dose-response models describing

270 the dose-dependent effects of peginterferon α-2a and ribavirin:

271 $$\varepsilon = \frac{Dose_{PEG}}{ED_{50_{PEG}} + Dose_{PEG}} \qquad (5)$$

272 $$\rho = \frac{Dose_{RBV}}{ED_{50_{RBV}} + Dose_{RBV}} \qquad (6)$$

273 where $Dose_{PEG}$ is the weekly subcutaneous dose of peginterferon α-2a and $ED_{50_{PEG}}$ is

274 the estimated weekly dose of peginterferon α-2a resulting in a 50% inhibition of the

275 virion production. Similarly, $Dose_{RBV}$ is the daily dose of ribavirin per kg body weight

276 and $ED_{50_{RBV}}$ is the estimated daily dose in mg/kg rendering 50% of the virions non-

277 infectious. $Dose_{RBV}$ and $ED_{50_{RBV}}$ were expressed as mg/kg as ribavirin is dosed by body

278 weight and ribavirin in mg/kg has been previously found to be a prognostic factor for

279 SVR (34).

280 The implementation of a *cure*/viral eradication boundary represents a milestone

281 contribution in enabling linking the complexity and diversity of clinically observed

282 Hepatitis C viral kinetics to SVR. The *cure* boundary was based on the assumption that

12

283   virion production (p) should cease when all infected cells are cleared, i.e., when there is

284   less that 1 infected cell in the total plasma and extracellular fluid volume of

285   approximately $13.5 \cdot 10^3$ mL. At the time point at which treatment anti-viral effect drove

286   the system to less than one infected hepatocyte, the virion production p was set to zero

287   (*off* state), resulting in a model *cure*/SVR [**Supplementary** text note 1 online (35)].

288   Exploratory simulations without this additional model component of *cure* predicted

289   rapid viral load return to baseline in all CHC patients when treatment was stopped

290   [**Supplementary** text note 1 online (35)], while in reality the virus is eradicated after

291   the current standard treatment of care in the majority of Gn1 infected patients and

292   approximately half of the HCV G1 patients and approximately (5).

293   A fundamental parameter of the viral kinetic model is the estimated basic reproduction

294   number (R_0) [**Supplementary** text note 2 online (18)]. Previously, it was shown that the

295   reproduction number in the presence of an inhibitor (R_T) is (*36*):

296   $$R_T = R_0 \cdot (1 - \varepsilon_T) \tag{8}$$

297   where ε_T is the total treatment-induced inhibition of the virion production. As infection

298   in the presence of an inhibitor has been shown to be cleared when $R_T < 1$ (36), ε_T

299   combined with R_0 are thus important predictors for a successful drug therapy. For this

300   reason, our model was parameterized in terms of R_0, by using the following equation for

301   R_0 (18):

302   $$R_0 = \frac{p \cdot \beta \cdot s}{c \cdot \delta \cdot d} \tag{9}$$

303   Finally, drug-effect after stopping treatment was described by an exponential decay

304   function ($e^{-K \cdot t}$, **Figure 2**), where K is the estimated antiviral-effect decay constant and t

305   the time from the end of treatment. Without the inclusion of this exponential decay

306   function, the viral load in relapsing patients after stopping therapy appeared to return

307   too rapidly to pre-treatment values

308

309   **Model assumptions**

310   Currently available data did not allow the estimation of all parameters of the declared

311   viral kinetic model due to issues of mathematical identifiability. For this reason, a

312   number of system/physiological parameters were fixed to biologically justifiable values.

313   The maximum number of hepatocytes present in an individual liver was assumed to be

314   $2.50 \cdot 10^{11}$ hepatocytes (37). As HCV RNA is distributed in plasma and extracellular

315   fluids with a volume of approximately $13.5 \cdot 10^3$ mL (38), the maximum number of

316   hepatocytes (T_{max}) was assumed to be $18.5 \cdot 10^6$ cells·mL^{-1} (12). Assuming a hepatocyte

317   turnover in a healthy liver of 300 days (39), the death rate of target cells (d) was set to

318   $1/300$ day^{-1}, and therefrom ($T_{max} \cdot d$) the production of new hepatocytes in the absence of

319   liver disease (s) could be assumed to be $61.7 \cdot 10^3$ cells·mL^{-1} days^{-1} (12). Estimated

320   proliferation rates were set to be equal across infected and uninfected hepatocytes due to

321   a lack of direct information to the contrary.

322   Non-linear mixed effects models comprise of a combination of fixed and random

323   effects. Individual parameters (PAR_i) in such a model are assumed to be log-normally

324   distributed and can be described by:

325   $PAR_i = \theta \cdot e^{\eta_i}$ (7)

326   where, subscript i denotes individual, the fixed effects parameter θ represents the

327   median (typical) value of the parameter in the population, and η_i is the random effect

328   accounting for the individual difference from the typical value. The η_i values are

329   assumed to be normally distributed in the population with a mean of zero and an

330 estimated variance of ω^2. Individual parameter estimates are used to predict the viral

331 load in an individual i at a certain point in time j ($V_{pred,ij}$). The measured viral load data

332 ($V_{obs,ij}$) were $\log_{10}$-transformed for the analysis in order to be able to handle the wide

333 range of viral load observations, and an additive residual error model was used for the

334 $\log_{10}$-transfomed viral load data:

335 $$log_{10} V_{obs,ij} = log_{10} V_{pred,ij} + \varepsilon_{ij} \tag{8}$$

336 The ε_{ij} values are assumed to be normally distributed with a mean of zero and an

337 estimated variance σ^2. The ω^2 quantifies the inter-individual variability (IIV) and the σ^2

338 quantifies the residual variability.

339 Estimated fixed effects parameters were R_0, p, c, δ, liver proliferation rate r

340 [**Supplementary** text note 3 online (17)], $ED_{50_{PEG}}$, $ED_{50_{RBV}}$ and K. IIV was incorporated

341 on the parameters R_0, c, δ and $ED_{50_{PEG}}$.

342

343 **Parameter estimation**

344 Population parameters of our HCV viral kinetic model were estimated using MLE by

345 the SAEM algorithm for hierarchical nonlinear mixed effects model analysis (40,41).

346 Individual parameters were obtained by computing for each individual patient the so-

347 called Maximum A Posteriori (MAP) esimate, which maximizes the conditional

348 distribution of the individual parameters using the MLE of the population parameters

349 computed previously with the SAEM algorithm (40). SAEM is a powerful algorithm for

350 MLE in complex models, including dynamic models defined by a system of ODE's.

351 Furthermore, the left-censored data are properly handled by the extended SAEM

352 algorithm for MLE as described by Samson *et al.* (22). The extended SAEM algorithm

353 for MLE is implemented in the *MONOLIX* software, available on the author's website

354 (16). We used version 2.4 of *MONOLIX*.

355

356 **Model evaluation and qualification**

357 Goodness of fit was assessed by the method of simulating from the final model and re-

358 fitting (23). Since by definition, the proposed model does not characterize SVR directly,

359 but SVR is derived from crossing the model *cure* boundary, the predictive performance

360 of the model in correctly classifying patients into SVR or non-SVR, which is considered

361 one of the core utilities of the model, could be assessed by calculating the sensitivity

362 and specificity (42,43) without confounding bias. The predictive performance of the

363 model was assessed by a model evaluation procedure using the design and data of a

364 large clinical trial not included in the model building dataset. In this trial, 180 μg

365 peginterferon α-2a was administered once weekly for 48 weeks, alone or in

366 combination with daily 1,000 or 1,200 mg ribavirin (4). Dropout rates in the simulated

367 cohort were matched to historical data by random assignment and defining dropouts as

368 non-SVR. The uncertainty of the observed SVR rates was quantified by 400 bootstrap

369 samples and compared to observed SVR rates in the trial.

370

371 **ACKNOWLEDGMENTS**

376 assistance, and Sharon Lim and Marlene Hering for help in the preparation of this

377 manuscript.

378

REFERENCES AND NOTES

1   World Health Organization. Hepatitis C. Available at
     http://www.who.int/mediacentre/factsheets/fs164/en/ Last accessed 15 September
     2008.

2   National Institutes of Health, Hepatology 36, S3 (2002).

3   Strader DB, Wright T, Thomas DL, Seeff LB; American Association for the Study
     of Liver Diseases.   Diagnosis, management, and treatment of hepatitis C.
     Hepatology. 2004 Apr;39(4):1147-71.

4   Fried MW, Shiffman ML, Reddy KR, Smith C, Marinos G, Gonçales FL Jr,
     Häussinger D, Diago M, Carosi G, Dhumeaux D, Craxi A, Lin A, Hoffman J, Yu J.
     Peginterferon alfa-2a plus ribavirin for chronic hepatitis C virus infection. N Engl
     J Med. 2002 Sep 26;347(13):975-82.

5   Hadziyannis SJ, Sette H Jr, Morgan TR, Balan V, Diago M, Marcellin P, Ramadori
     G, Bodenheimer H Jr, Bernstein D, Rizzetto M, Zeuzem S, Pockros PJ, Lin A,
     Ackrill AM; PEGASYS International Study Group.   Peginterferon-alpha2a and
     ribavirin combination therapy in chronic hepatitis C: a randomized study of
     treatment duration and ribavirin dose. Ann Intern Med. 2004 Mar 2;140(5):346-55.

6   Zein NN, Rakela J, Krawitt EL, Reddy KR, Tominaga T, Persing DH. Hepatitis C
     virus genotypes in the United States: epidemiology, pathogenicity, and response to
     interferon therapy. Collaborative Study Group.   Ann Intern Med. 1996 Oct
     15;125(8):634-9.

7   Dixit NM, Layden-Almer JE, Layden TJ, Perelson AS. Modelling how ribavirin
     improves interferon response rates in hepatitis C virus infection. Nature. 2004 Dec
     16;432(7019):922-4.

8   Perelson AS, Herrmann E, Micol F, Zeuzem S.   New kinetic models for the hepatitis C virus. Hepatology. 2005 Oct;42(4):749-54.

9   Neumann AU, Lam NP, Dahari H, Gretch DR, Wiley TE, Layden TJ, Perelson AS. Hepatitis C viral dynamics in vivo and the antiviral efficacy of interferon-alpha therapy. Science. 1998 Oct 2;282(5386):103-7

10   Perelson AS, Neumann AU, Markowitz M, Leonard JM, Ho DD. HIV-1 dynamics in vivo: virion clearance rate, infected cell life-span, and viral generation time. Science. 1996 Mar 15;271(5255):1582-6.

11   Wei X, Ghosh SK, Taylor ME, Johnson VA, Emini EA, Deutsch P, Lifson JD, Bonhoeffer S, Nowak MA, Hahn BH, et al.   Viral dynamics in human immunodeficiency virus type 1 infection. Nature. 1995 Jan 12;373(6510):117-22.

12   Colombatto P, Civitano L, Oliveri F, Coco B, Ciccorossi P, Flichman D, Campa M, Bonino F, Brunetto MR. Sustained response to interferon-ribavirin combination therapy predicted by a model of hepatitis C virus dynamics using both HCV RNA and alanine aminotransferase. Antivir Ther. 2003 Dec;8(6):519-30.

13   Zeuzem S.   The kinetics of hepatitis C virus infection.   Clin Liver Dis. 2001 Nov;5(4):917-30

14   Layden JE, Layden TJ. Viral kinetics of hepatitis C: new insights and remaining limitations. Hepatology. 2002 Apr;35(4):967-70.

15   Layden-Almer JE, Cotler SJ, Layden TJ. Viral kinetics in the treatment of chronic hepatitis C. J Viral Hepat. 2006 Aug;13(8):499-504

16   http://www.monolix.org/

17   Dahari H, Lo A, Ribeiro RM, Perelson AS. Modeling hepatitis C virus dynamics: liver regeneration and critical drug efficacy. J Theor Biol. 2007;247(2):371-81.

18   Callaway DS, Perelson AS. HIV-1 infection and low steady state viral loads. Bull Math Biol. 2002 Jan;64(1):29-64.

19   Pomfret EA, Pomposelli JJ, Gordon FD, Erbay N, Lyn Price L, Lewis WD, Jenkins RL. Liver regeneration and surgical outcome in donors of right-lobe liver grafts. Transplantation. 2003 Jul 15;76(1):5-10.

20   Neumann AU, Lam NP, Dahari H, Davidian M, Wiley TE, Mika BP, Perelson AS, Layden TJ. Differences in viral dynamics between genotypes 1 and 2 of hepatitis C virus. J Infect Dis. 2000 Jul;182(1):28-35. Epub 2000 Jul 6.

21   US FDA label information of Pegasys and Copegus. Available at: http://www.fda.gov

22   Samson A, Lavielle M, Mentré F. Extension of the SAEM algorithm to left-censored data in nonlinear mixed-effects model: Application to HIV dynamics model. Computational Statistics & Data Analysis. Volume 51, Issue 3, 1 December 2006, Pages 1562-1574.

23   Karlsson MO, Savic RM. Diagnosing model diagnostics. Clin Pharmacol Ther. 2007;82:17-20.

24   Bernardin F, Tobler L, Walsh I, Williams JD, Busch M, Delwart E. Clearance of hepatitis C virus RNA from the peripheral blood mononuclear cells of blood donors who spontaneously or therapeutically control their plasma viremia. Hepatology. 2008 May;47(5):1446-52.

25   Wodarz D. Mathematical models of immune effector responses to viral infections: virus control versus the development of pathology. J. Comp. Appl. Math. 2005; 184:301-319.

26   Dienstag JL, McHutchison JG. American Gastroenterological Association technical review on the management of hepatitis C. Gastroenterology 2006; 130:231–64)

27   Strader DB, Wright T, Thomas DL, Seeff LB.   Diagnosis, management, and treatment of hepatitis C. Hepatology. 2004; 39:1147–71.

28   Samson A, Lavielle M, Mentré F.   The SAEM algorithm for group comparison tests in longitudinal data analysis based on non-linear mixed-effects model. Stat Med. 2007 Nov 30;26(27):4860-75.

29   Heathcote EJ, Shiffman ML, Cooksley WG, Dusheiko GM, Lee SS, Balart L, Reindollar R, Reddy RK, Wright TL, Lin A, Hoffman J, De Pamphilis J. Peginterferon alfa-2a in patients with chronic hepatitis C and cirrhosis. N Engl J Med. 2000 Dec 7;343(23):1673-80.

30   Zeuzem S, Feinman SV, Rasenack J, Heathcote EJ, Lai MY, Gane E, O'Grady J, Reichen J, Diago M, Lin A, Hoffman J, Brunda MJ. Peginterferon alfa-2a in patients with chronic hepatitis C. N Engl J Med. 2007;357(2):124-34.

31   Reddy KR, Wright TL, Pockros PJ, Shiffman M, Everson G, Reindollar R, Fried MW, Purdum PP, Jensen D, Smith C, Lee WM, Boyer TD, Lin A, Pedder S, DePamphilis J.   Efficacy and safety of pegylated (40-kd) interferon alfa-2a compared with interferon alfa-2a in noncirrhotic patients with chronic hepatitis C. Hepatology 2001;33(2)433-8.

32   Pockros PJ, Carithers R, Desmond P, Dhumeaux D, Fried MW, Marcellin P, Shiffman ML, Minuk G, Reddy KR, Reindollar RW, Lin A, Brunda MJ; PEGASYS International Study Group. Efficacy and safety of two-dose regimens of peginterferon alpha-2a compared with interferon alpha-2a in chronic hepatitis C: a multicenter, randomized controlled trial.   Am J Gastroenterol. 2004 Jul;99(7):1298-305.

33   Lee SC, Antony A, Lee N, Leibow J, Yang JQ, Soviero S, Gutekunst K, Rosenstraus M.   Improved version 2.0 qualitative and quantitative AMPLICOR reverse transcription-PCR tests for hepatitis C virus RNA: calibration to international units, enhanced genotype reactivity, and performance characteristics. J Clin Microbiol. 2000 Nov;38(11):4171-9.

34   Snoeck E, Wade JR, Duff F, Lamb M, Jorga K.   Predicting sustained virological response and anaemia in chronic hepatitis C patients treated with peginterferon alfa-2a (40KD) plus ribavirin. Br J Clin Pharmacol. 2006;62(6):699-709.

35   CPT Supplementary online material

36   Jacqmin P *et al.,* submitted for publication in J. Pharmacokinet. Pharmacodyn.

37   Sherlock S, Dooley J. in Disease of the Liver and Biliary system (Blackwell Science, 1998), pp 8.

38   Liou TC, Chang TT, Young KC, Lin XZ, Lin CY, Wu HL.   Detection of HCV RNA in saliva, urine, seminal fluid and ascites. J Med Virol. 1992;37(3), 203-9.

39   Mc Sween RNM, Anthony PP, Scheuer PJ,   Pathology of the Liver – Second edition Churchill Livingstone, 1987.

40   Delyon B, Lavielle M, Moulines E.   Covergence of a stochastic approximation version of the EM algorithm. Ann. Statist. 1999; 27: 94-128.

41   Kuhn E, Laveille M.   Maximum likelihood estimation in nonlinear mixed effects models. Comput. Statist. Data Anal. 2005; 1020-1038.

42   Altman DG, Bland JM.   Statistical notes: diagnostic tests 1: sensitivity and specificity. BMJ. 1994; 308: 1552.

43   Bishop YM, Fienberg SE, PW Holland. Discrete multivariate analysis: theory and

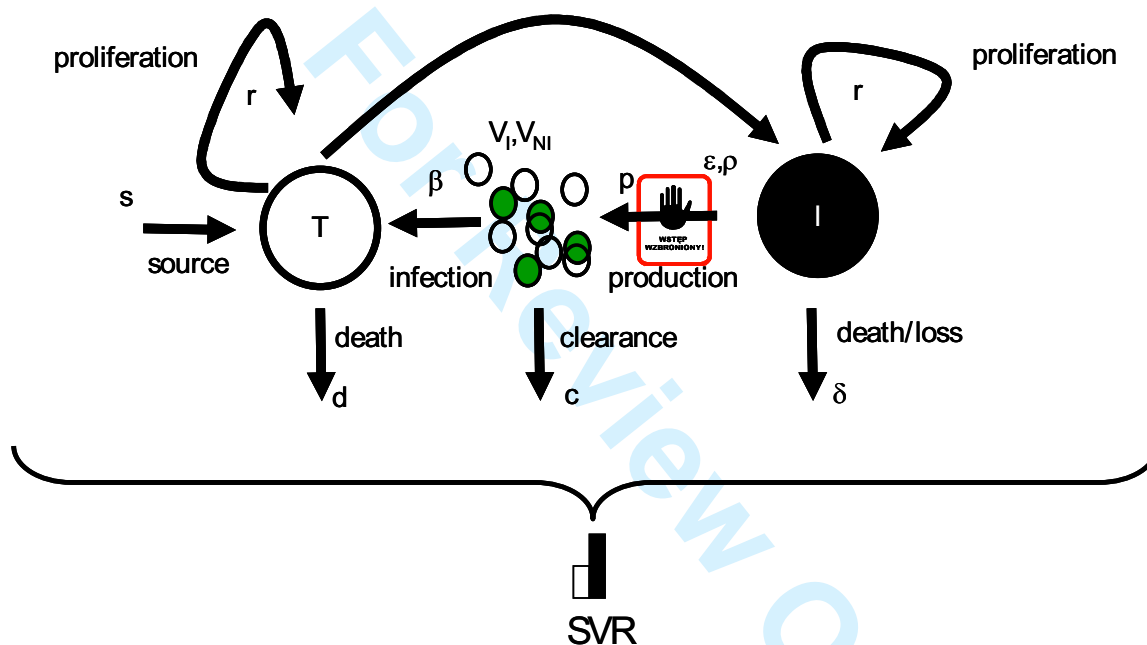practice. The MIT Press, 1977.

FIGURES AND TABLES

Figure 1. Representation of the extended HCV viral kinetic model. Infectious HCV virions (V_I) infect target cells (T), creating productively infected hepatocytes (I). Uninfected hepatocytes (T) are produced at rate s and die at rate d. Infected hepatocytes die at rate δ. A density dependent proliferation of hepatocytes (r) is assumed. Infectious (V_I) and non-infectious (V_{NI}) virions are produced at rate p and cleared at rate c. Peginterferon α-2a dose-dependently inhibits the production of new virions (ε), and ribavirin dose-dependently renders a fraction of newly produced virions non-infectious (ρ). SVR, defined as an undetectable viral load at 24 weeks after treatment completion, is the primary clinical endpoint desired to be predicted in the treatment of Hepatitis C.
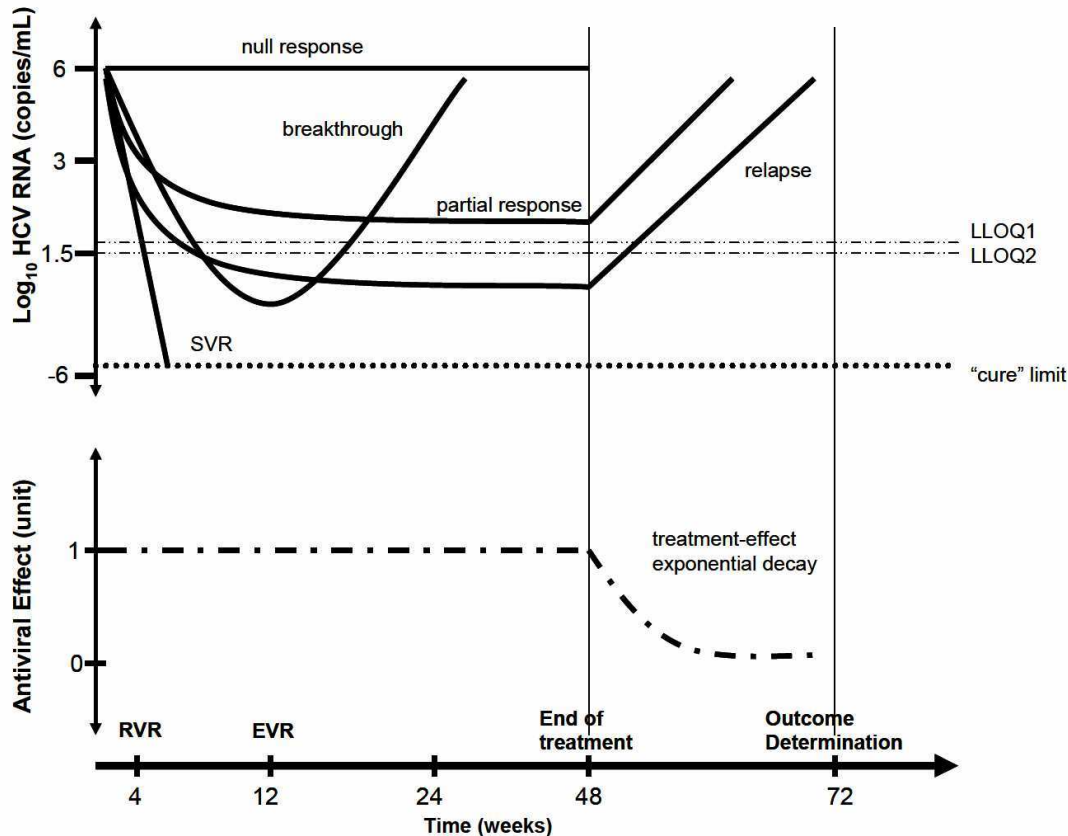
Figure 2. The viral kinetic model characterizes the complexity and diversity of clinically observed HCV viral kinetics in Hepatitis C virus patients treated with peginterferon α-2a alone or in combination with ribavirin, and links the kinetics to clinical outcome. This is achieved by the implementation of a viral eradication *cure* boundary and incorporation of left-censored data, previously largely excluded from analysis, from simultaneous analysis of a wide spectrum of peginterferon α-2a ± ribavirin treatment regimens from 2,100 patients. RVR and EVR are rapid virologic response and early virologic response, respectively.
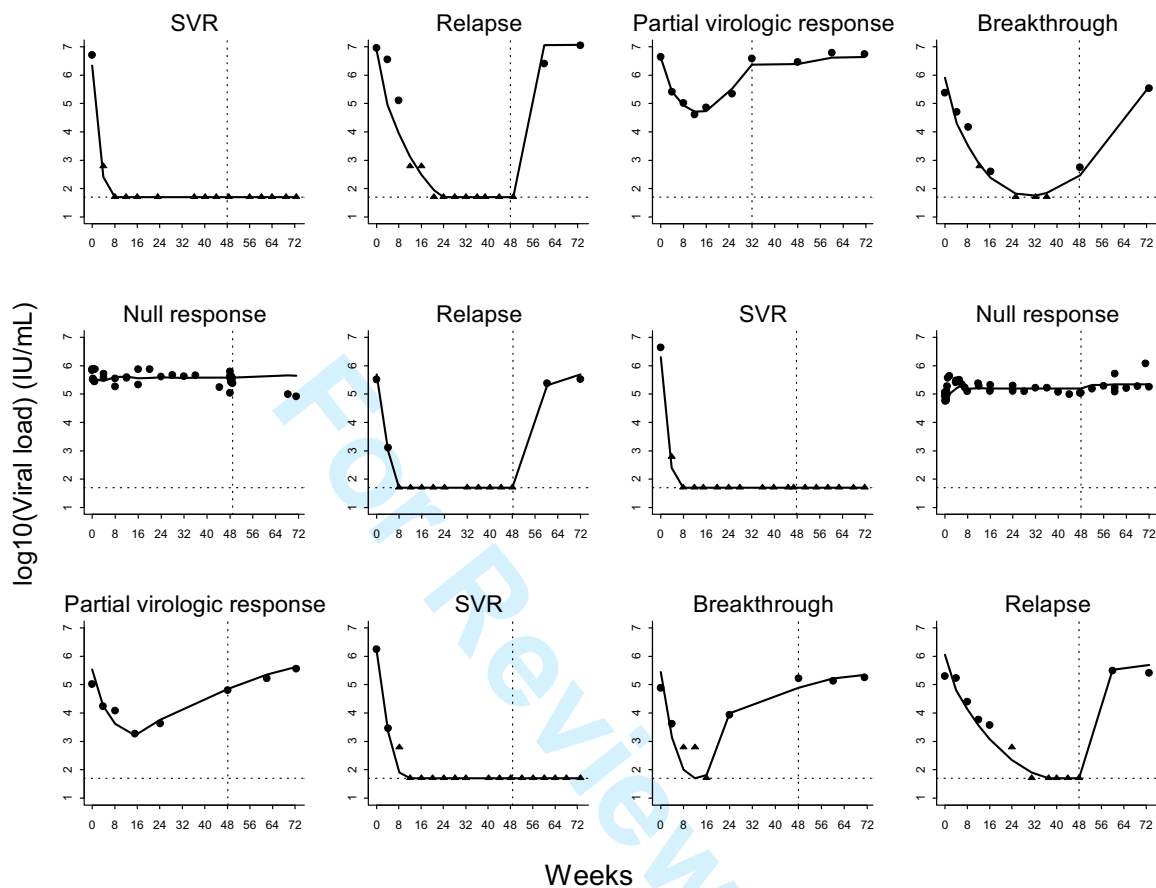
25

Figure 3. Observed and model-predicted long-term viral load profiles in 12 representative CHC patients. Solid lines are the fits of the model to the individual viral load data which are either detectable (closed circles) or below the LLOQ of 50 IU/mL (closed triangles). Dotted horizontal lines show the LLOQ of the assay. Dotted vertical lines indicate the end of treatment. Our HCV viral kinetic model is able to describe all the typical phenomena observed after long-term therapy such as null response (no change in viral load), partial virologic response (initial decrease followed by increase during treatment), *breakthrough* during therapy (non-detectable viral load followed by increase during treatment), *relapse* after therapy (non-detectable viral load at the end of therapy followed by an increase during the treatment-free follow-up period), and SVR (non-detectable viral load at 24 weeks after end of therapy).
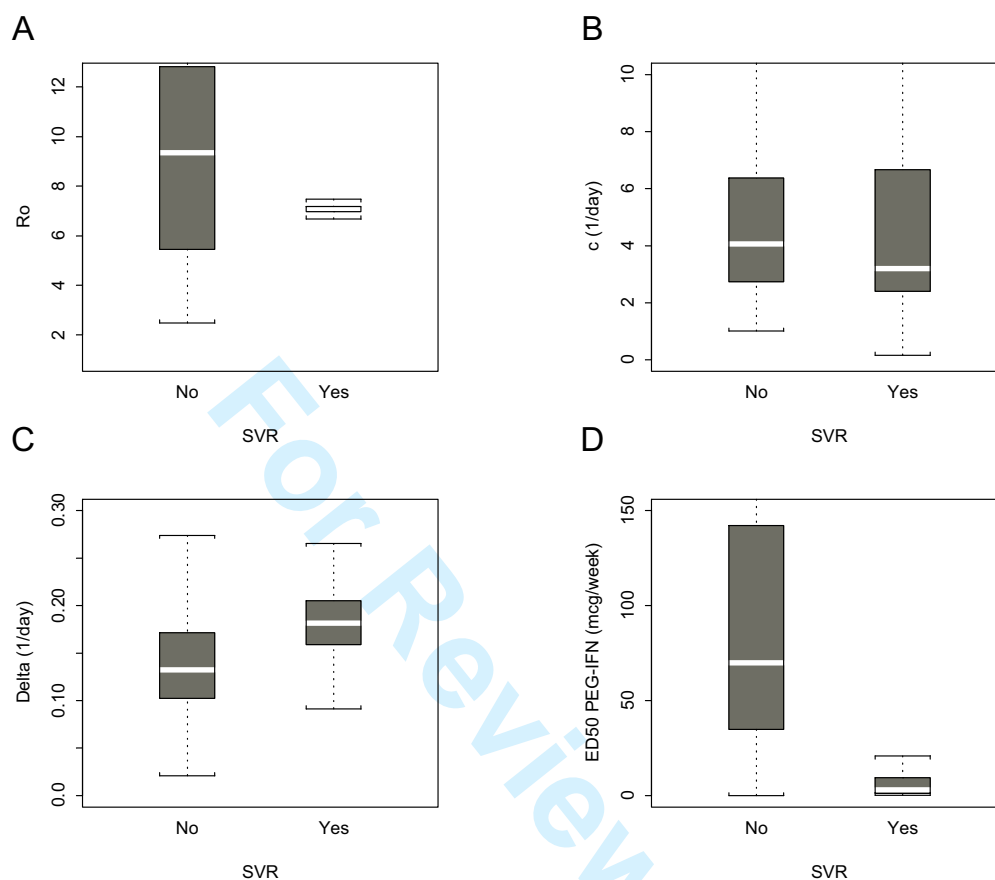
A

B

C

D

Figure 4. Boxplots of the individual HCV viral kinetic model parameters as split by patient outcome (i.e. SVR (n = 974) *versus* non-SVR (n = 1,126) patients). The basic reproduction number (R_0) is generally higher and more variable in patients without an SVR (**A**). The free virion clearance rate (*c*) is not different between patients with and without an SVR (**B**). The infected cell death rate (*δ*) is generally higher in patients with an SVR (**C**), and the effectiveness of peginterferon α-2a in inhibiting the production of new virions is generally higher in patients with an SVR (**D**).
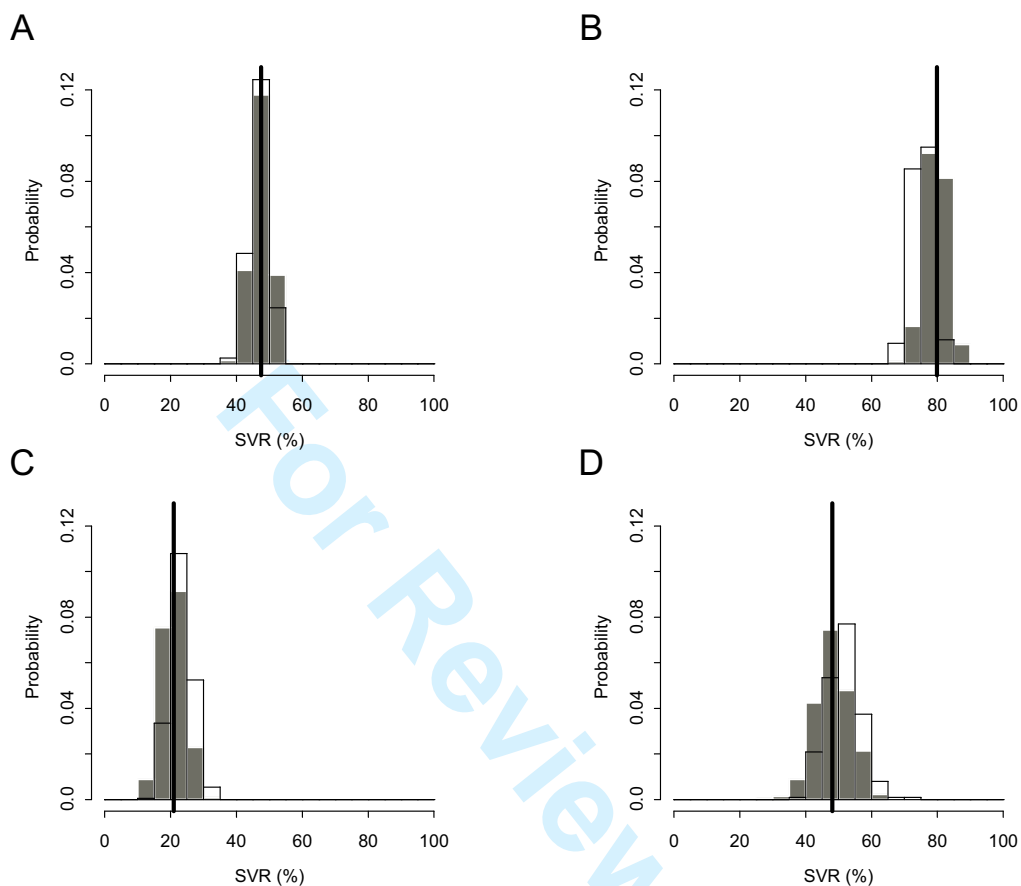
Figure 5. Observed (black vertical lines) and model predicted SVR rates (transparent histogram) of the phase-III study by Fried *et al.* (*4*), investigating 180 μg peginterferon α-2a once weekly for 48 weeks given alone or in combination with daily 1,000 or 1,200 mg ribavirin. Dropouts have been taken into account in the predictions by randomly assigning patients as dropout and defining them as non-SVR. The uncertainty of the observed SVR rates was quantified by 400 bootstrap samples (grey histograms). The observed SVR rate in 297 HCV G1 patients receiving combination therapy falls within the range of model predicted SVR rates (**A**). The observed SVR rate in 154 HCV Gn1 patients receiving combination therapy also falls within the range of model predicted SVR rates (**B**). The observed SVR rate in 143 HCV G1 patients receiving monotherapy of peginterferon α-2a falls within the range of model predicted SVR rates (**C**). Finally, also the observed SVR rate in 77 HCV Gn1 patients receiving monotherapy of peginterferon α-2a falls within the range of model predicted SVR rates (**D**).

Table 1. Population parameters of the HCV viral kinetic model fitted to the individual long-term viral load profiles of 2,100 CHC patients receiving chronic treatment of peginterferon α-2a alone or in combination with ribavirin[*]. The upper part of the table represents the fixed parameters according to our assumptions, the middle part are system-specific parameters and the lower part are the drug-specific parameters. The SE reflects the precision of the estimated parameters and IIV represents the inter-individual variability (**Supplementary** text note 5 online).

Parameter	Description	Unit	Typical value	SE (%CV)[***]	IIV (%CV)
T_{max}	Total amount of hepatocytes per mL	hepatocytes·mL^{-1}	$18.5 \cdot 10^6$		
s	Hepatocyte production rate	hepatocytes·mL^{-1}·day^{-1}	$61.7 \cdot 10^3$		
d	Hepatocyte death rate constant	day^{-1}	0.003		
r	Hepatocyte proliferation rate constant	day^{-1}	0.00562	22	
R_0[****]	Basic reproductive number		7.15	9	137
p	Virion production rate	virions·hepatocyte^{-1} day^{-1}	25.1	15	
c	Virion elimination rate constant	day^{-1}	4.53	15	120
$\delta_{HCV\,non-1}$	Infected cell death rate constant (HCVGn1)	day^{-1}	0.192	16	58[*]
δ_{HCV-1}	Infected cell death rate constant (HCV G1)	day^{-1}	0.139	3	58[*]
$ED_{50_{PEG\ HCV\ non-1}}$	ED_{50} of peginterferon α-2a (HCV Gn1)	μg·week^{-1}	1.19	17	281[*]
$ED_{50_{PEG\ HCV-1}}$	ED_{50} of peginterferon α-2a (HCV genotype-1)	μg·week^{-1}	20.9	10	281[*]
$ED_{50_{RBV}}$	ED_{50} of ribavirin	mg·kg^{-1}·day^{-1}	14.4	18	
K	Anti-viral effect decay constant	day^{-1}	0.0238	13	
σ^2	Residual error		0.260	1	

[*]   47% received monotherapy of peginterferon α-2a at a weekly subcutaneous dose of 45 μg (20 patients), 90 μg (114 patients), 135 μg (210 patients), 180 μg (596 patients) or 270 μg (38 patients). The CHC patients receiving combination therapy were administered a subcutaneous dose of 180 μg/week peginterferon α-2a and a daily dose of 800 mg or 1,000/1,200 mg ribavirin. Almost all patients (93%) received 24 weeks of treatment or more, and 61% of CHC patients received 48 weeks of treatment or more.

[**]   Assumed to be similar between HCV genotype-1 and non-1 infected patients.

[***]   As T_{max}, s and d were fixed, no SE is provided.

[****] R_0 is defined as the number of newly infected cells that arise from one infected cell when almost all cells are uninfected and has therefore no units.

Supplementary text note 1: additional model component for HCV virion eradication

Exploratory simulations were undertaken based on the HCV viral kinetic model as described by equations 1-6 of the manuscript. An evaluation of the simulated viral load profiles of the CHC patient population revealed that the viral load in all patients rapidly returned back to baseline within approximately 4 to 8 weeks after stopping the 48-week treatment (**Figure S1**). This implies that an SVR cannot be described without adding a model component for HCV virion eradication. A subsequent simulation based on the same model where only one infected cell (*I*) remained at the end of treatment showed again a rapid return to baseline within approximately 4 weeks (**Figure S2**). As the virion production *p* should cease when all infected hepatocytes are cleared, parameter *p* was set to zero (**off** state) during the model fitting procedure when the number of infected hepatocytes crossed the < 1 cell or < 1/13500 cells·mL^{-1} *cure* boundary condition.

Supplementary text note 2: basic reproduction number (R_0)

The basic reproduction number of an infection is defined as the number of newly infected hepatocytes that arise from one infected cell when almost all cells are infected, i.e. prior to treatment initiation (*S1*). When $R_0 < 1$, the infection will be spontaneously cleared in the long run. But if $R_0 > 1$, the infection will be able to expand. When $R_0 = 1$, the infection will not be cleared or expand but remain at some quasi-disease equilibrium. Using a simple PK-PD model for proliferative systems, it can be shown that the reproduction number in the presence of an inhibitor of the virion production (R_T) is (*S2*):

$$R_T = R_0 \cdot (1 - \varepsilon_T) \tag{1}$$

where ε_T is the total treatment-induced inhibition of the virion production. The infection in the presence of an inhibitor will die out in case $R_T < 1$ (*S2*). R_0 thus carries information on the status of infection, whereas R_T carries information about treatment effect and the likelihood of *cure*.

Simulations based on our HCV viral kinetic model confirmed the previous findings based on the simple PK-PD model for proliferative systems (**Figure S3**). The total drug effectiveness ε_T combined with R_0 are thus important predictors for successful drug therapy. For this reason, our model was parameterized in terms of R_0, by using the following equation for R_0 (*S3*):

$$R_0 = \frac{p \cdot \beta \cdot s}{c \cdot \delta \cdot d} \tag{2}$$

In our model, the parameters d and s are assumed to be respectively $1/300$ day^{-1} and $61.7 \cdot 10^3$ cells·mL^{-1} days^{-1}, whereas R_0, c, p and δ are estimated so that the *de novo* infection rate constant β can be calculated.

Supplementary text note 3: liver proliferation rate (r)

The liver is a unique organ as it self-heals by regeneration as opposed to repair. The exact cellular and molecular mechanisms of liver regeneration are still not yet fully understood (*S4,S5*). The Neumann HCV viral kinetic model was extended with a density-dependent liver proliferation term to describe the liver regeneration (*S6*). For liver regeneration in healthy liver donors, the liver regrowth can be described in a similar way:

$$\frac{dT}{dt} = s + r \cdot T \cdot \left(1 - \frac{T}{T_{max}}\right) - d \cdot T \tag{3}$$

T represents the number of hepatocytes in cells·mL^{-1}. The maximum number of hepatocytes present in an individual liver (T_{max}) is assumed to be $18.5 \cdot 10^6$ cells·mL^{-1}.

The death rate of hepatocytes (d) is assumed to be 1/300 day^{-1}, and the production of new hepatocytes (s) is thus $61.7 \cdot 10^3$ cells·mL^{-1} days^{-1} from steady-state assumptions. Simulations of the liver regeneration based on the above mentioned equation and the model estimated a maximum liver proliferation rate (r) of 0.006 day^{-1}, and also revealed a rapid initial liver regrowth (**Figure S4**). For a donor remnant liver volume of 50%, the total liver volume was predicted to be approximately 89% after 360 days. This predicted total liver volume matched well with the increase in original liver volume as measured over a 1-year time period in 51 donors who provided right-lobe liver grafts (*S7*).

Supplementary text note 4: goodness of fit assessment

As anticipated, a diagnostic plot of the observed viral load values (DV) *versus* the population predictions (PRED) [**Figure S5**] is neither intuitive nor very informative. Because of the wide diversity of the various viral load profiles (**Figure 3** of manuscript), the population based diagnostic plots have limited meaning for the assessment of the goodness of fit. In principle, the population prediction would be the same for a null-responder, a breakthrough patient, a patient having a relapse and a SVR patient. This implies that conditional estimates of the model parameters should be taken into account for model diagnostics based on population predictions to make sense. A plot of the population weighted residuals (WRES) *versus* PRED [**Figure S6**] shows a certain pattern which can be well explained by comparing the time course of the population predicted viral load with the individual viral load values. In order to assess the expected pattern of the DV *versus* PRED and WRES *versus* PRED plots of our model, mirror plots were created in which "observations" were simulated three times from the final model and these "observations" were subsequently re-fitted to create the PRED and WRES plots based on the parameters used in the simulation (**Figures S5-**

S6). The patterns of the PRED- and WRES-based diagnostics for the observed and simulated data were similar, implying that the observed pattern of these two population-based diagnostic plots matched with the expected pattern for our model (*S*8).

As population based diagnostics were not very infomative, goodness of fit was assessed based on diagnostic plots for the individual predictions (IPRED) [**Figure S7**], individual weighted residuals (IWRES) [**Figure S8**] and the absolute values of the individual weighted residuals (|IWRES|) [**Figure S9**]. The ε–shrinkage was calculated to be 9%, implying that individual predictions can be used as a reliable diagnostic (*S*8). Mirror plots were also created for IPRED, IWRES and |IWRES| (**Figures S7-S9**). The patterns of the goodness of fit plots for IPRED, IWRES and |IWRES| for the observed and simulated data were similar, implying that no model misspecification was evident from the diagnostic (*S*8), and thus indicating that the individual viral load profiles are well described by the model. In addition, the goodness of fit plot of |IWRES| *versus* IPRED indicates that the residual error model was appropriate.

The η–shrinkage was calculated to be 39% for the basic reproduction number (R_0), 17% for the free virion clearance rate (c), 31% for the infected cell death rate (δ) and 34% for $ED_{50_{PEG}}$. As anticipated, the relatively high shrinkage values are driven by the typical viral load profiles of the different patient categories (i.e. null-responders, breakthrough patients, relapsing patients and patients having an SVR). For instance, the shrinkage of δ, describing the second phase of the viral load decay, was only 4% in breakthrough patients and 17% in patients having a relapse. These two patient categories generally have a relatively slow decay of the viral load so that the individual values of δ can be well estimated. SVR-patient viral load decline was generally characterized by a fast decay so that the second phase is not always visible, while null or partial responding

patients, had a relatively flat profile, and the δ estimate was more shrunken towards the population mean.

Supplementary text note 5: performance of model-based SVR classification

Statistical measures of the performance of the SVR classification by the HCV viral kinetic model were obtained by comparing the SVR classification (SVR or non-SVR) based on the model to the observed SVR classification in each individual patient present in the database of 2,100 CHC patients. Since by definition, the proposed model does not characterize SVR directly, but SVR is derived from crossing the model *cure* boundary, the performance of the model related to correctly classifying patients could be assessed by calculating the sensitivity and specificity based on individual predictions of HCV RNA including those obtained post-treatment (9,10) without confounding bias. A total of 941 patients were found to be True Positive (observed SVR and model-predicted SVR), and 1,119 CHC patients were found to be True Negative (observed non-SVR and model-predicted non-SVR) [**Table S1**]. A total of 33 patients were found to be False Negative (observed SVR but model-predicted non-SVR), and 7 patients were found to be False Positive (observed non-SVR but model-predicted SVR). Based on these numbers, the sensitivity and specificity was calculated to be 96.6% and 99.4%, respectively. Although the difference in the number of correctly and incorrectly classified individuals is quite convincing, it should be noted that the sensitivity and specificity are positively biased as the rows and columns of **Table S1** are not fully independent. The positive predictive value (PPV) and negative predictive value (NPV) was calculated to be 99.3% and 97.1%, respectively. In calculating these two statistics, it is assumed that the prevalence in the population at large is similar.
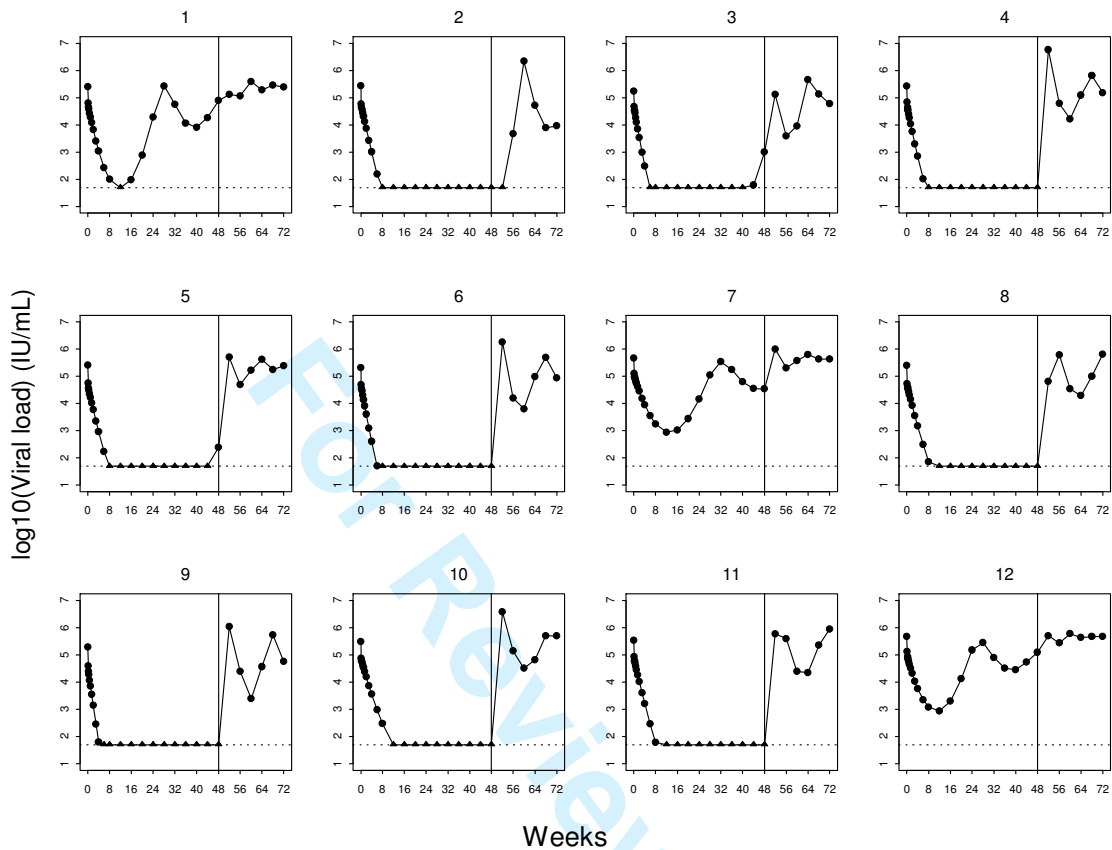
Figure S1. Simulated long-term viral load profiles in 12 CHC patients receiving a 48-week treatment. Viral load profiles were simulated assuming $R_0 = 8$, $p = 6$ virions·cell^{-1}·day^{-1}, $c = 3$ day^{-1}, $\delta = 0.2$ day^{-1}, $r = 0.005$ day^{-1} and an inhibition of the virion production of 80%. IIV was assumed to be 40 %CV for R_0 and 20% CV for all other parameters. Simulated individual viral load data are either detectable (closed circles) or below the LLOQ of 50 IU/mL (closed triangles). Dotted horizontal lines show the LLOQ of the assay. Vertical lines indicate the end of treatment at 48 weeks.
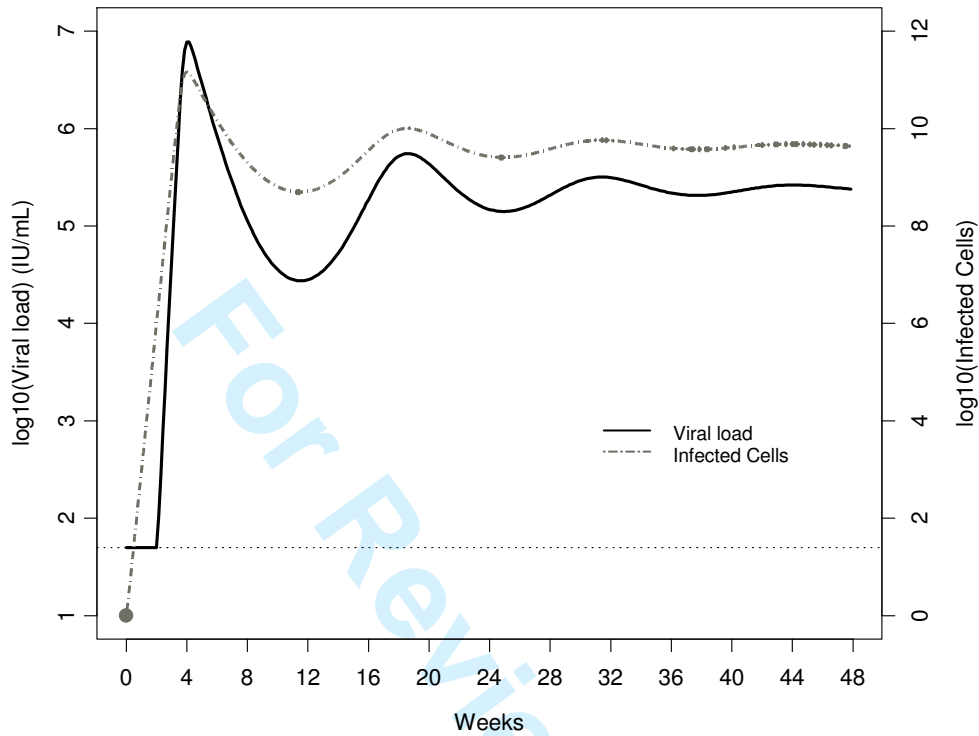
Figure S2. Simulated HCV viral load (black line) and simulated number of infected hepatocytes (grey dashed line) with only one infected cell remained at the end of treatment. The simulation was performed with $R_0 = 8$, $p = 6$ virions·cell^{-1}·day^{-1}, $c = 3$ day^{-1}, $\delta = 0.2$ day^{-1} and liver proliferation rate $r = 0.005$ day^{-1}. The dotted horizontal lines show the LLOQ of the assay of 50 IU/mL.
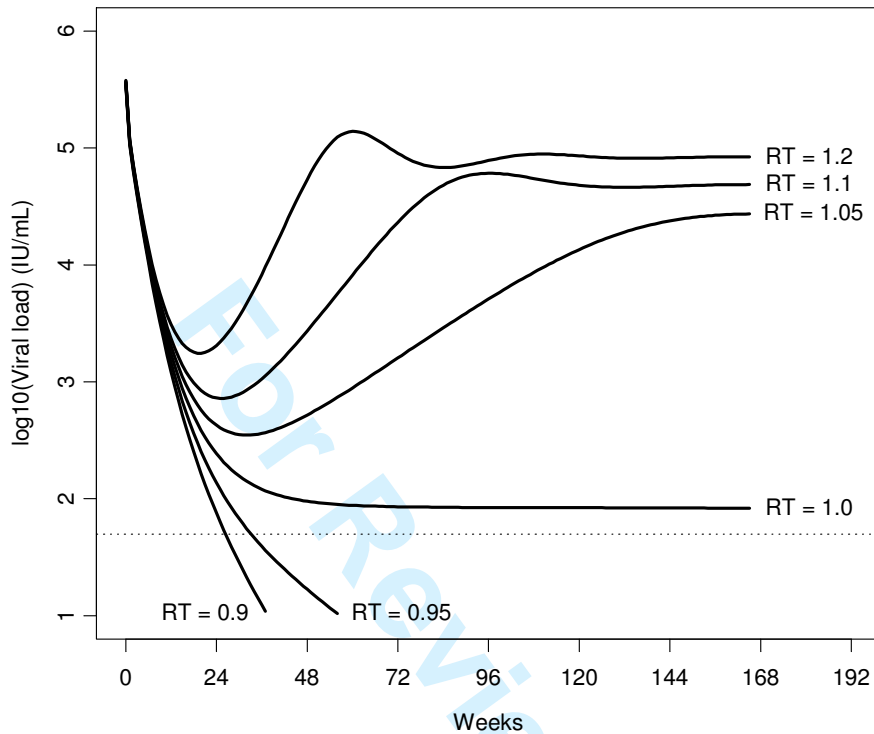
Figure S3. Simulated HCV viral load profiles during a 192-week antiviral therapy resulting in a continuous 50% inhibition of the virion production ($\varepsilon = 0.5$). Simulations were performed with $p = 6$ virions·cell^{-1}·day^{-1}, $c = 3$ day^{-1}, $\delta = 0.16$ day^{-1} and $r = 0.01$ day^{-1}. The dotted horizontal line shows the LLOQ of the assay of 50 IU/mL. The basic reproductive number (R_0) was assumed to be 2.4, 2.2, 2.1, 2.0, 1.9 and 1.8, respectively resulting in a basic reproduction number in the presence of a 50% inhibition of the virion production (R_T) of 1.2, 1.1, 1.05, 1.0, 0.95 and 0.9 (see equation S1). Simulations confirmed that when $R_T < 1$, the infection will be cleared in the long run. But if $R_T > 1$, the infection will expand. When $R_T = 1$, the infection will not be cleared or expand but remain at some quasi-disease equilibrium.
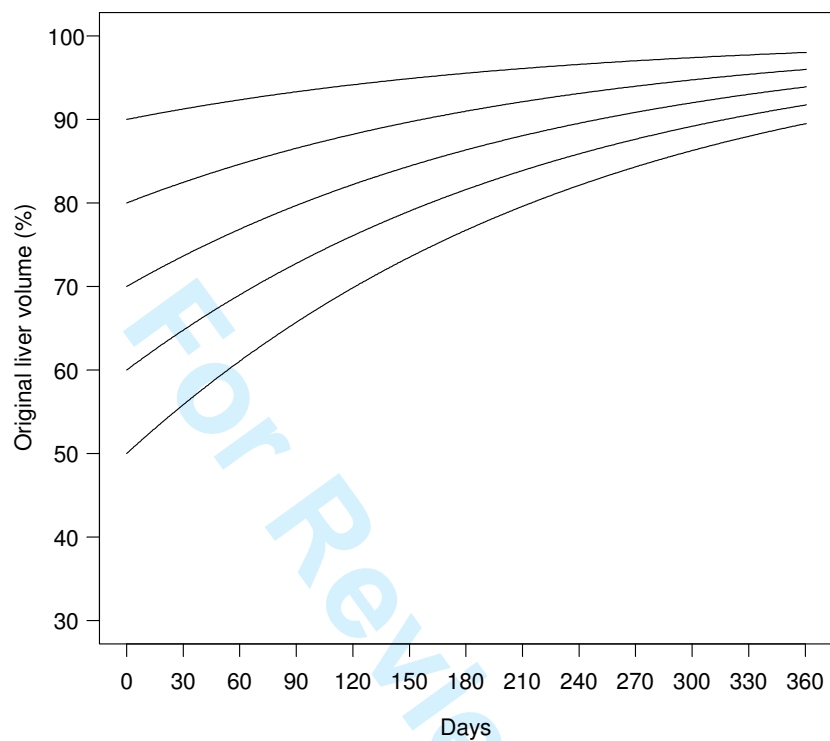
Figure S4. Simulated liver regeneration after a donor remnant liver volume of 50%, 60%, 70%, 80% and 90% of the original total liver volume. Simulations were performed with the model estimated maximum liver proliferation rate (r) of 0.006 day^{-1}.
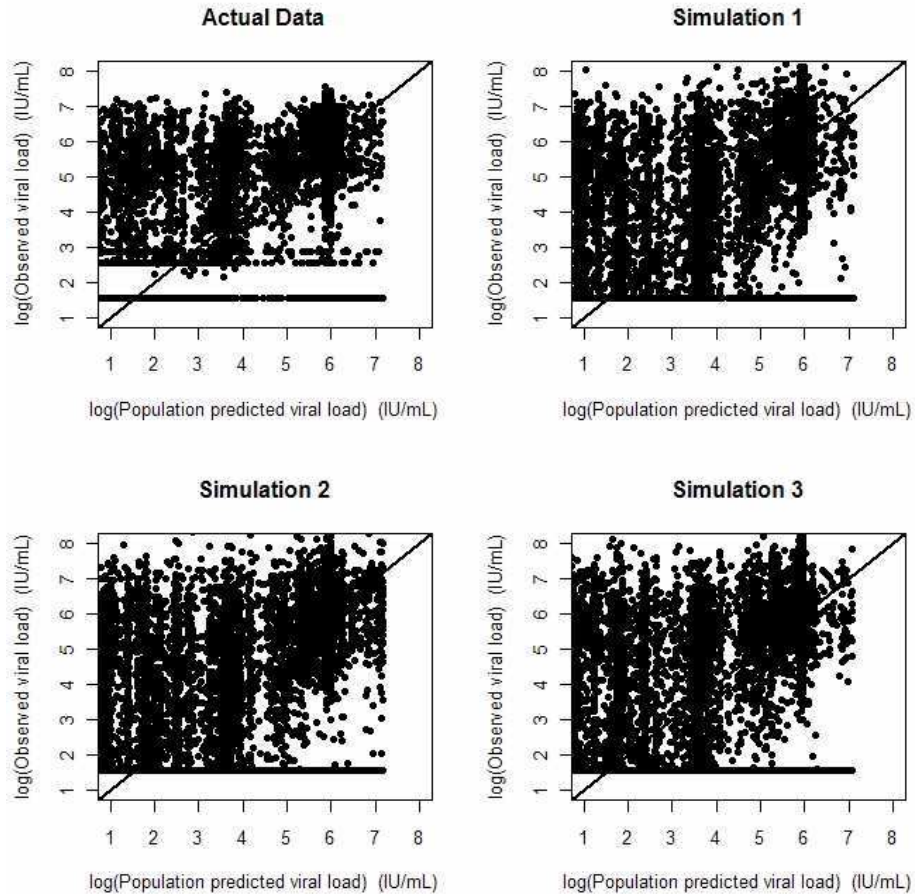
Figure S5. Mirror plot of the observed *versus* population predictions (PRED) for the HCV viral kinetic model fitted to the actual data (upper left panel) and when all "observations" are simulated three times with the same model as is used to calculate the individual predictions (upper right panel and lower panels). The predicted values are based on the estimated parameter values. The solid black line is the line of identity which should go through the middle of the data. Simulations were undertaken with an LLOQ of 50 IU/mL explaining the presence of more lower "observed" values in the simulations.
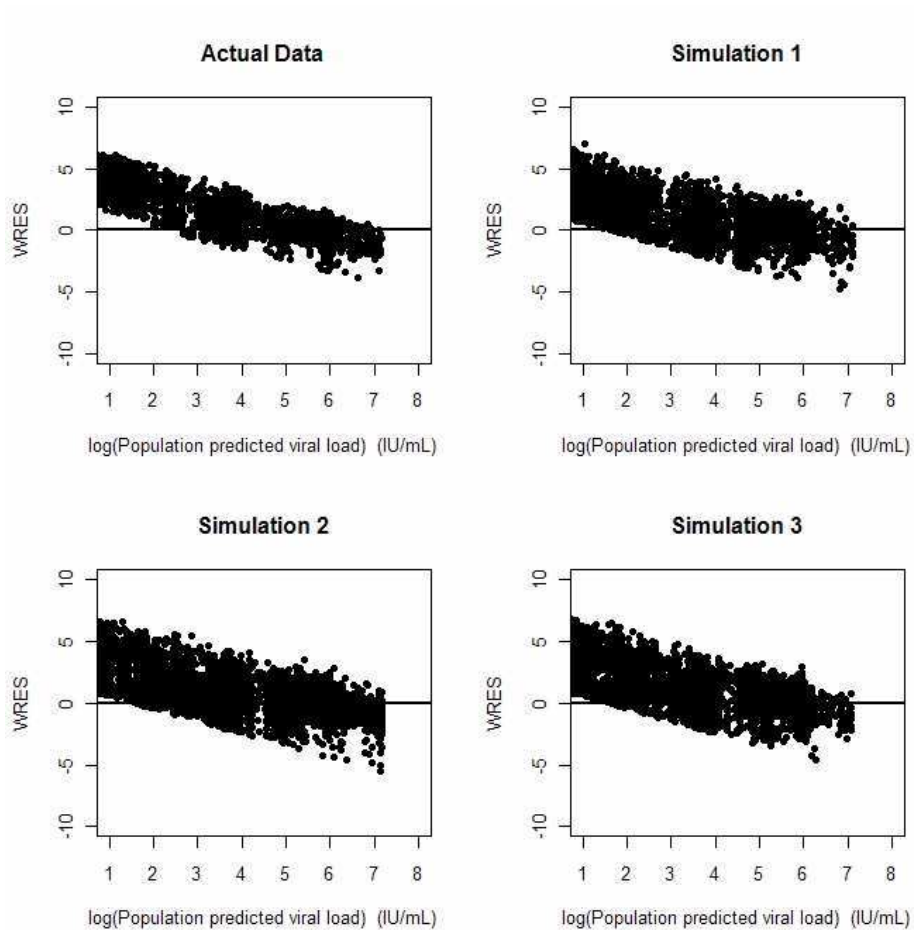
Figure S6. Mirror plot of the weighted residuals (WRES) *versus* population predictions (PRED) for the HCV viral kinetic model fitted to the actual data (upper left panel) and when all "observations" are simulated three times with the same model as is used to calculate the WRES (upper right panel and lower panels). The solid black line is the zero line.
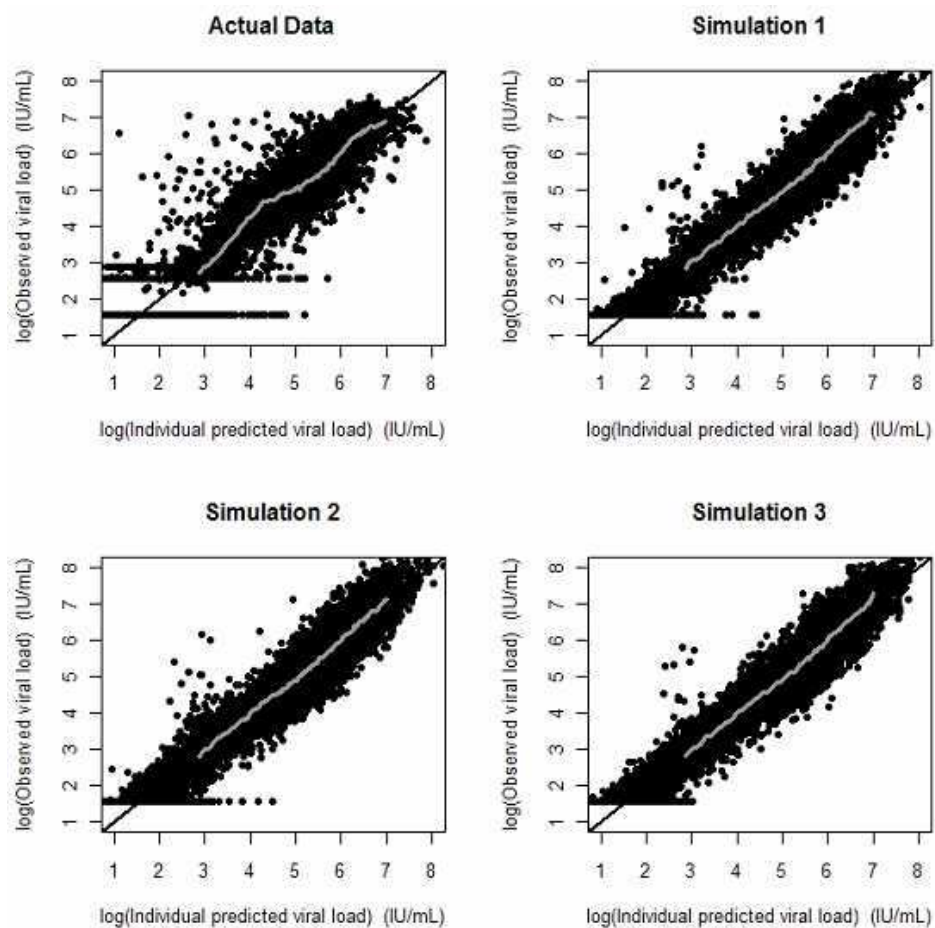
Figure S7. Mirror plot of the observed *versus* individual predictions (IPRED) for the HCV viral kinetic model fitted to the actual data (upper left panel) and when all "observations" are simulated three times with the same model as is used to calculate the individual predictions (upper right panel and lower panels). The predicted values are based on the estimated parameter values. The grey line represents a smooth through the data. The solid black line is the line of identity which should go through the middle of the data. Simulations were undertaken with an LLOQ of 50 IU/mL explaining the presence of more lower "observed" and IPRED values in the simulations.
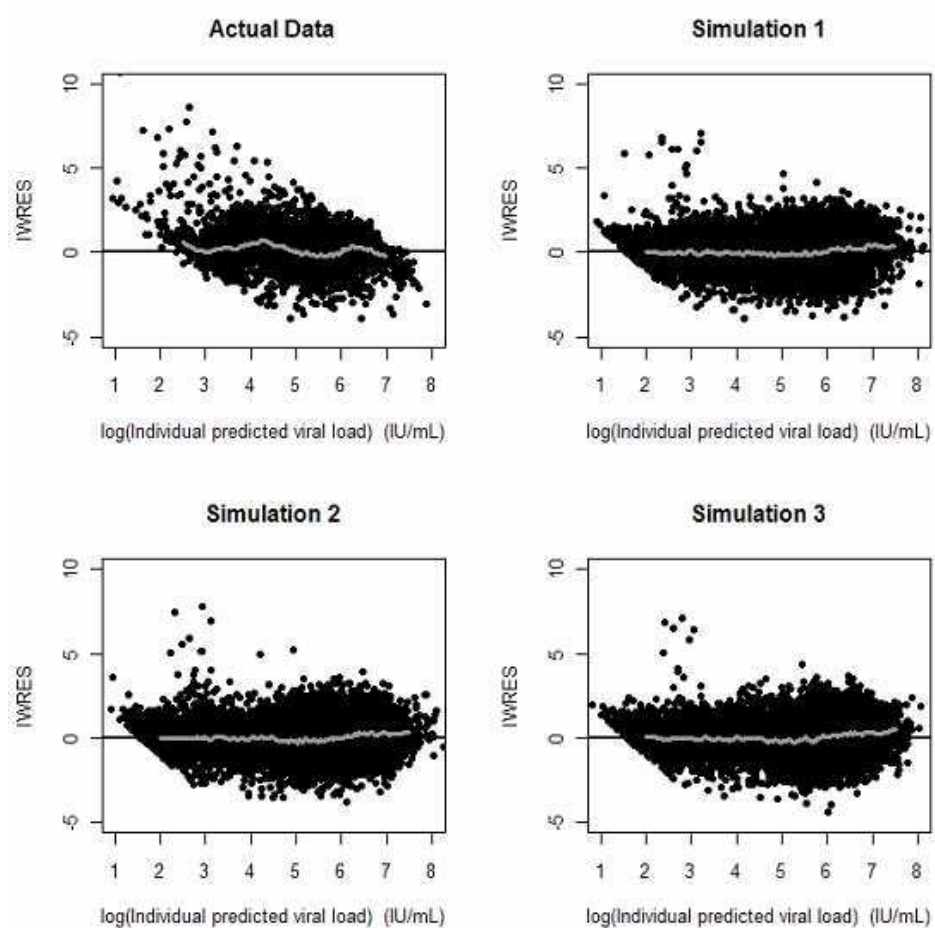
Figure S8. Mirror plot of the individual weighted residuals (IWRES) *versus* individual predictions (IPRED) for the HCV viral kinetic model fitted to the actual data (upper left panel) and when all "observations" are simulated three times with the same model as is used to calculate the IWRES (upper right panel and lower panels). The grey line represents a smooth through the data. The solid black line is the zero line around which the values of IWRES should be randomly and densely scattered. Simulations were undertaken with an LLOQ of 50 IU/mL explaining the presence of more lower IPRED values in the simulations. Some higher IWRES values are present for small IPRED values based on the actual data. However, these data points present only a minor fraction of the overall data.
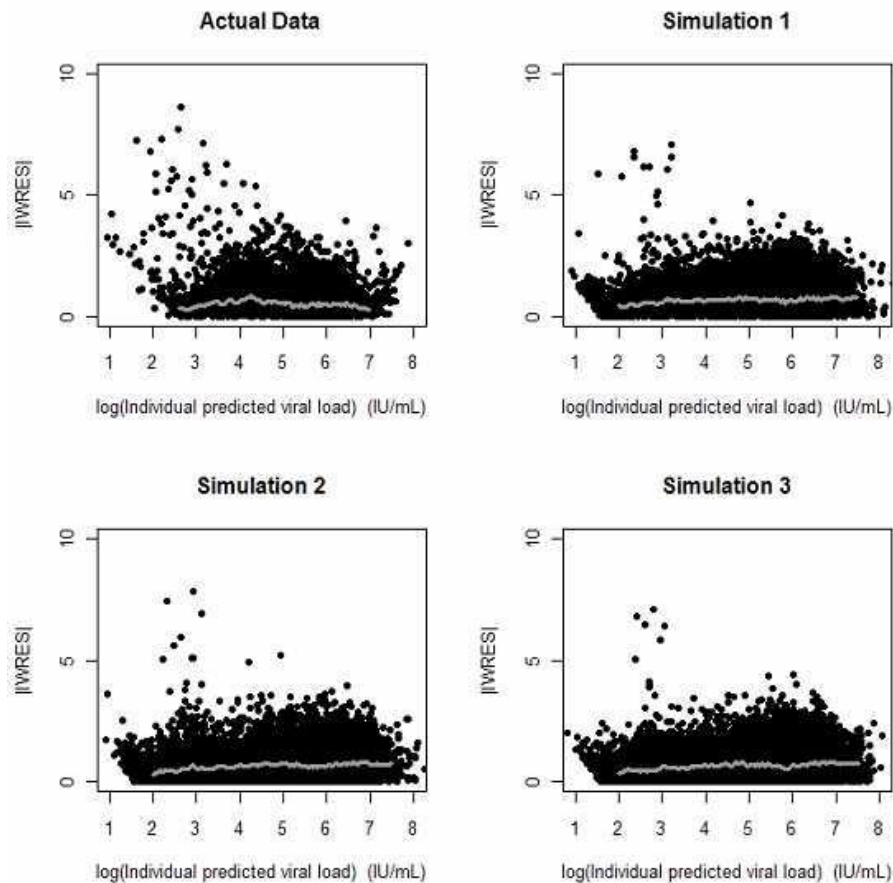
Figure S9. Mirror plot of the absolute values of the individual weighted residuals (|IWRES|) *versus* individual predictions for the HCV viral kinetic model fitted to the actual data (upper left panel) and when all "observations" are simulated three times with the same model as is used to calculate the |IWRES| (upper right panel and lower panels). Simulations were undertaken with an LLOQ of 50 IU/mL explaining the presence of more lower IPRED values in the simulations. Some higher |IWRES| values are present for small IPRED values based on the actual data. However, these data points present only a minor fraction of the overall data.

Table S1. Calculation of the sensitivity, specificity, positive predictive value (PPV) and negative predictive value (NPV) for the model-based classification of CHC patients into SVR or non-SVR.

		Observed SVR		Total
		SVR = 1	SVR = 0	
Fitted SVR	SVR = 1	True Positive 941	False Positive 7	948 PPV[3] = 99.3%
	SVR = 0	False Negative 33	True Negative 1119	1152 NPV[4] = 97.1%
	Total	974 Sensitivity[1] = 96.6%	1,126 Specificity[2] = 99.4%	2,100

[1]Sensitivity is calculated as 941 divided by 974 and expressed as %.

[2]Specificity is calculated as 1,119 divided by 1,126 and expressed as %.

[3]Positive predicted value (PPV) is calculated as 941 divided by 948 and expressed as %.

[4]Negative predictive value (NPV) is calculated as 1,119 divided by 1,152 and expressed as %.

References for supporting online material

1   Heffernan JM, Smith RJ, Wahl LM. Perspectives on the basic reproductive ratio.
       J R Soc Interface. 2005 Sep 22;2(4):281-93.

2   Jacqmin P *et al.,* submitted for publication in J. Pharmacokinet. Pharmacodyn.

3   Callaway DS, Perelson AS. HIV-1 infection and low steady state viral loads.
       Bull Math Biol. 2002 Jan;64(1):29-64.

4   Michalopoulos GK, DeFrances MC. Liver regeneration. Science. 1997 Apr
       4;276(5309):60-6.

5   Khan AZ, Mudan SS. Liver regeneration : mechanisms, mysteries and more.
       ANZ J. Surg. 2007;**77**:9-14.

6   Dahari H, Lo A, Ribeiro RM, Perelson AS. Modeling hepatitis C virus dynamics:
       liver regeneration and critical drug efficacy.   J Theor Biol. 2007 Jul
       21;247(2):371-81. Epub 2007 Mar 14.

7   Pomfret EA, Pomposelli JJ, Gordon FD, Erbay N, Lyn Price L, Lewis WD,
       Jenkins RL. Liver regeneration and surgical outcome in donors of right-lobe liver
       grafts. Transplantation. 2003 Jul 15;76(1):5-10.

8   Karlsson MO, Savic RM. Diagnosing model diagnostics. Clin Pharmacol Ther
       2007;82(1):17-20.

9   Altman DG, Bland JM. Statistical notes: diagnostic tests 1: sensitivity and
       specificity. BMJ. 1994; 308: 1552.

10   Bishop YM, Fienberg SE, PW Holland. Discrete multivariate analysis: theory and
       practice. The MIT Press, 1977.